# Interferometric Synthetic Aperture Sonar in Pipeline Inspection

Roy Edgar Hansen, Torstein Olsmo Sæbø
and Hayden John Callow
Norwegian Defence Research Establishment (FFI)
P O Box 25, NO-2027 Kjeller, Norway
Roy-Edgar.Hansen@ffi.no; Torstein-Olsmo.Sabo@ffi.no;
Hayden-John.Callow@ffi.no

Per Espen Hagen
Kongsberg Maritime
P O Box 111, NO-3191 Horten, Norway
Per.Espen.Hagen@kongsberg.com

***Abstract*— Accurate and reliable inspection of subsea pipelines traditionally requires the use of multiple sensors, which again have different requirements for range and geometry. This makes pipeline inspection a time consuming and costly process. The use of high resolution synthetic aperture sonar (SAS) can potentially change this substantially. Current state of the art interferometric SAS systems offer very high resolution imagery and bathymetry over a very wide swath. Mounted on an autonomous underwater vehicle (AUV), such a system can provide highly detailed data sets of a pipeline with just one or two passes – either fully autonomously, or with operator supervision as desired. In June 2009, a Kongsberg Maritime HUGIN 1000-MR AUV equipped with a HISAS 1030 interferometric SAS performed such a pipeline inspection mission in Western Norway. The paper will show examples of the data recorded during the above mission.**

## I. Introduction

Interferometric synthetic aperture sonar (SAS) [1] provides the possibility to perform underwater mapping with very high resolution and at the same time obtain a large coverage rate [2]. We propose to use a high-resolution interferometric SAS for pipeline inspection. Pipeline inspection is usually performed by using a short-range sensor close to the pipeline, which gives limited information about the surroundings. By using an interferometric SAS, a large area including the pipeline can be mapped and imaged in one swath.

Fig. 1. The HUGIN 1000-MR AUV onboard the RNoN MCMV Hinnøy in august 2008.

Fig. 2. The HISAS 1030 wideband interferometric SAS.

Kongsberg Maritime and The Norwegian Defence Research Establishment (FFI) has developed a high-resolution interferometric SAS named HISAS 1030 [3], [4], along with an extensive processing tool named FOCUS [5]. In 2008 a HUGIN 1000-MR autonomous underwater vehicle (AUV) with HISAS-1030 was sold to the Royal Norwegian Navy (RNoN). Figure 1 shows the vehicle onboard the MCMV Hinnøy just before launch, and Figure 2 shows a closeup of the HISAS 1030 system. In June 2009 RNoN performed a survey outside the western coast of Norway with this vehicle, where main purpose of the mission was to survey an area with a pipeline, exposed, partly exposed and buried. The particular pipeline has a diameter of $12'' \approx 30\,\text{cm}$, and known position prior to the mission.

A pipeline inspection survey with imaging sonar may contain the following tasks [6]

- Detection of burial for exposed pipelines
- Detection of exposure for buried pipelines
- Detection of pipeline free span and estimation of span
- Detection of damages of pipelines
- Detection of buckling of pipelines
- Detection of debris near the pipeline

For long automated AUV surveys and short range sensors, tracking of the pipeline [7] might be mandatory. With the swath width of HISAS 1030 and the navigation accuracy of HUGIN 1000-MR AUV, tracking actually only becomes

Dette er en postprint-versjon/This is a postprint version.
DOI til publisert versjon/DOI to published version: 10.1109/OCEANSSYD.2010.5603518

important for multi-hour missions (given that the pipeline position is known). FFI has started a project to develop detection and tracking algorithms for pipeline tracking, with planned demonstrations at the end of 2010 and 2011.

In this paper, we focus on the sensor, interferometric SAS, and the particular benefits and challenges in inspection of the pipeline and the area around.

## II. Imaging concepts

On each side of the vehicle, the HISAS 1030 sensor contains two phased array receivers and a fully programmable vertical phased array transmitter [8]. In SAS-mode there is a limitation on the maximum displacement between pings, which again limits the maximum range [2], [9]. The data from this sensor can be used to produce different imaging products [10], as illustrated in Figure 3:

- The phased array receiver can be used to produce a 2D image per ping – a *sectorscan image*. The image then represents a snapshot in time, and the field of view is approximately 23° for HISAS 1030 operated at 100 kHz center frequency.
- The receiver array can be used to produce single or multiple range lines per ping – a *sidescan image*. Each range line represents each time instant (or ping), and the angular resolution (or angular spread into each pixel) is around 0.7°. The theoretical resolution is the same for sectorscan and sidescan at broadside.
- An image can be constructed by coherent combination of data from multiple pings into each pixel – a *synthetic aperture image*. In each pixel, the angular spread is equivalent to the sectorscan image [11], while the resolution is given by along-track element sizes [9], and the actual processing applied. A HISAS 1030 SAS image can have an angular resolution of 0.03° at 100 m range or better.

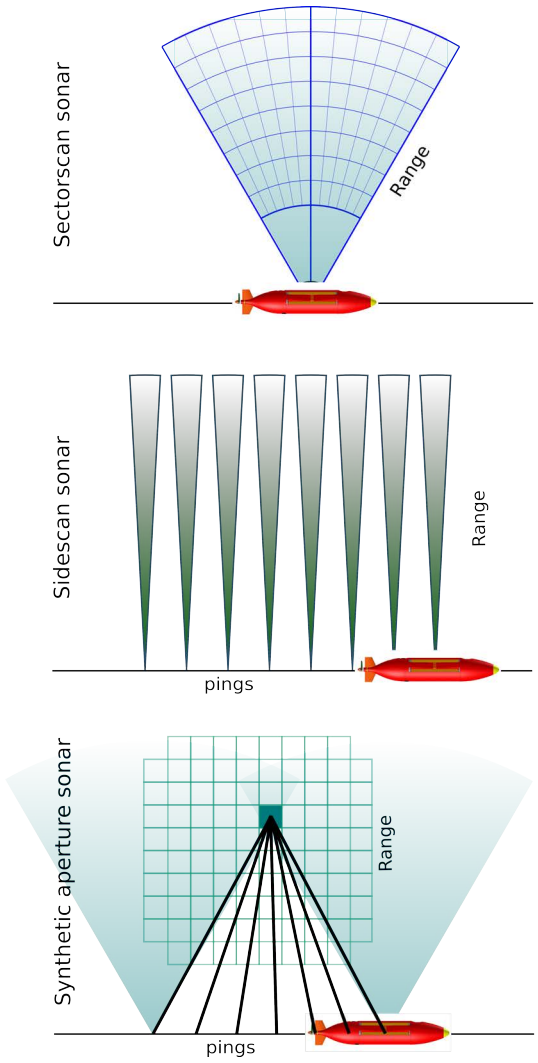


Fig. 3. Imaging concepts. Upper panel: Sectorscan image or 2D phased array image of one ping. Middle panel: Sidescan sonar image or stack of 1D range profiles. Lower panel: Synthetic aperture sonar or combination of many pings into each pixel.

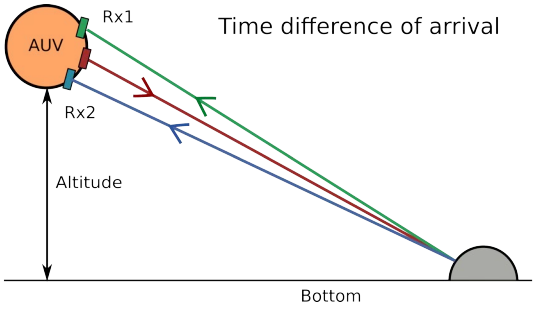


Fig. 4. The principle of interferometry is based on estimating the time difference of arrival to two vertically displaced receivers.

For all these image products, we use near field imaging (or dynamic focusing) [12]. HISAS 1030 is designed as a long baseline interferometer, with two vertically displaced receiver arrays on each side [3]. From this, the relative seafloor height, or bathymetry, can be calculated based on the estimated time difference of arrival on the receiver arrays [13]. This is illustrated in Figure 4. In order to produce ambiguity-free estimates of the seafloor height (or avoid phase wraps), HISAS 1030 uses large relative bandwidth.

## III. Data collection

Figure 5 shows an overwiew of a HUGIN mission outside the western coast of Norway. The color-coded bathymetry is estimated using interferometry on the HISAS-1030 data. The water depth varies from 200 m to 400 m in the test area. the tracks are shown in black and the pipeline in brown. In this paper we focus on two different areas from this mission: Area A and Area B are indicated by the two squares. Figure 6 shows a sidescan sonar image from one mission line from one of the sonars (one of the sides). Note that the pipeline is covered by gravel in several locations.

In Area B the AUV runs parallel to the pipeline at around 60 meters range to both sides. We have co-registered [14] data from the two sides and merged SAS images and SAS bathymetry. The results are presented in Section V. In Area

Dette er en postprint-versjon/This is a postprint version.
DOI til publisert versjon/DOI to published version: 10.1109/OCEANSSYD.2010.5603518

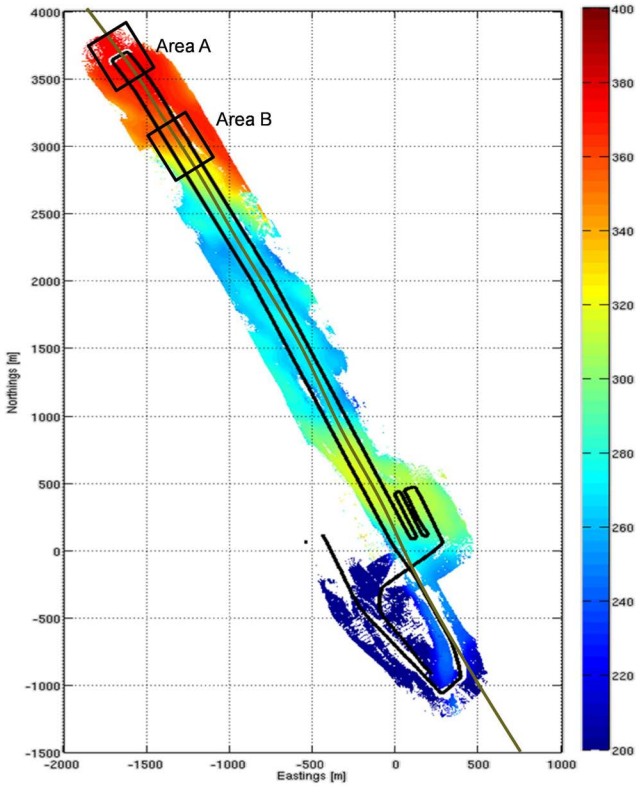


Fig. 5. Overview of the pipeline mission. The data are collected by the Royal Norwegian Navy.

A the AUV has run perpendicular to the pipeline and passed directly above it. Processed data from Area A are presented in Section VI. In Section VII we present results from shape estimation of the pipeline from both datasets.

Figure 7 shows an example SAS image from the pipeline mission. The image shows a $50 \times 100$ m scene, and the zoomed panel shows $10 \times 10$ m cutout. Note the very high resolution. The pipeline is exposed, partly buried and buried. The pipeline's surroundings are particularly important—external factors are responsible for many incidents of pipeline damage. Simple examples may be misplaced fishing trawls or an anchors which have been entangled to the pipeline or it can be a change in the landmass or underwater avalanches, which causes the pipeline to slide down a slope. Figure 8 shows an example where an anchor has been released nearby a pipeline and where there may be cause for a closer inspection.

## IV. Scattering geometry

Figure 9 shows some of the mechanisms involved in scattering of acoustic waves from an exposed cylinder (a pipeline) on the seafloor. A few simplified assumptions can be made:

- The specular reflection is the first arrival (closest range in the sonar image)
- If the pipeline is sufficiently smooth, the specular reflection will dominate the backscattered signal
- If the pipeline material is non-smooth (seen with the sonar), diffuse scattering (non-specular) will occur

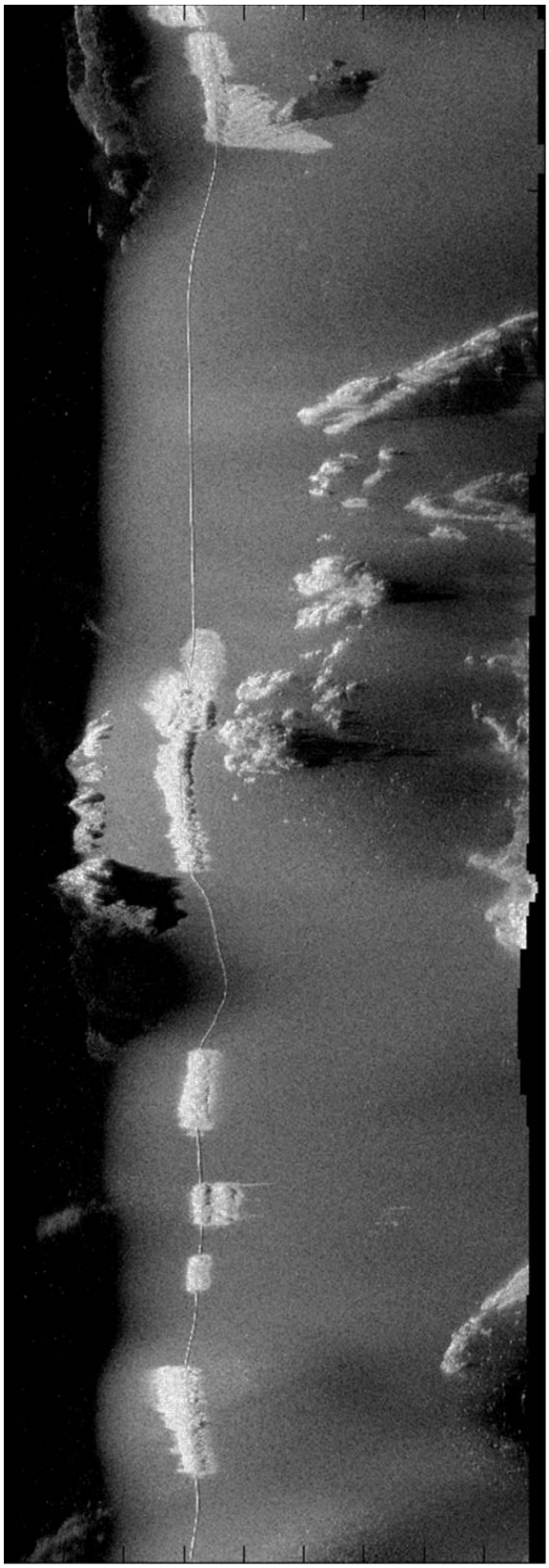

Fig. 6. Sidescan sonar image of the pipeline as a function of range and pings. The range is 0 m (left) to 180 m (right). The approximate distance travelled is 2000 m.

Dette er en postprint-versjon/This is a postprint version.
DOI til publisert versjon/DOI to published version: 10.1109/OCEANSSYD.2010.5603518

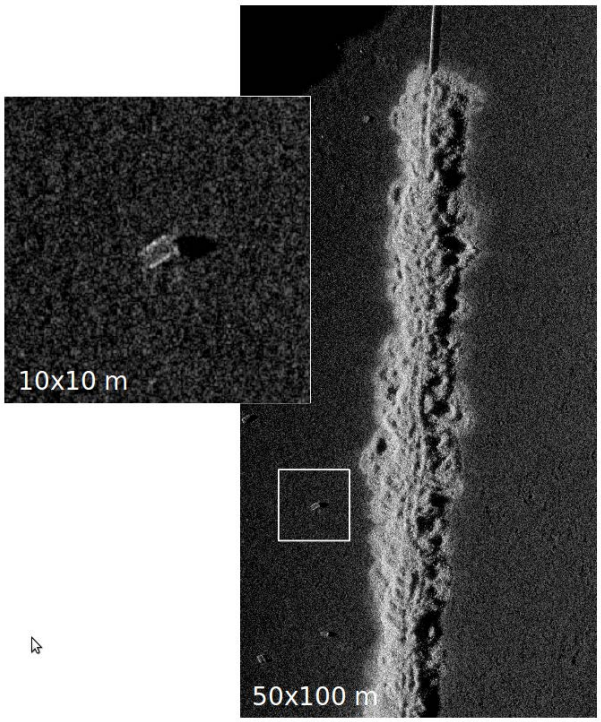


Fig. 7. Example SAS image of a 50 by 100 meters area from the pipeline mission. The cutout shows a small object, possibly a barrel.

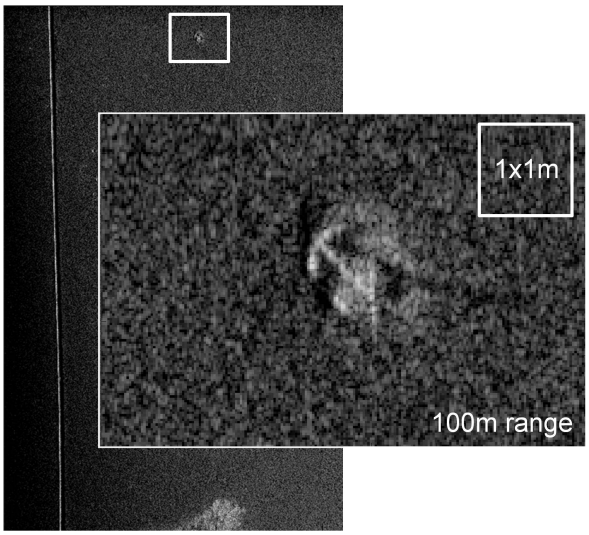


Fig. 8. Example of a SAS image of a 130 by 100 meters area. The large cutout has range from 40 meters (left) to 140 meters (right). The pipeline is located in the left part of the image. The zoom shows an anchor on the seafloor around 50 meters away from the pipeline.

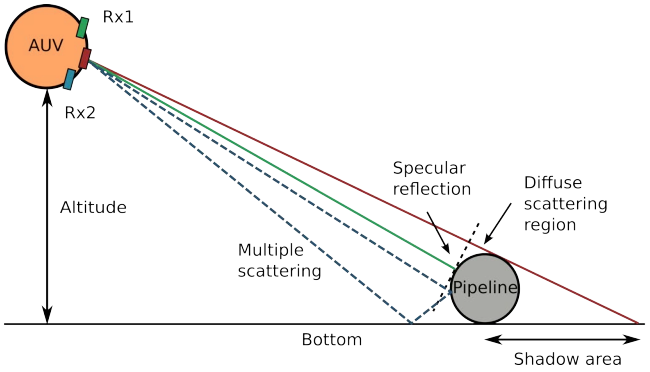


Fig. 9. Scattering geometry

- The top of the pipeline may not be observed since it requires diffuse scattering
- The acoustic signal may travel via the pipeline and then the seafloor, then into the receiver (multipath). In this case, the direction of arrival will be incorrect (i.e. incorrect bathymetry). The backscattered echo will also have a small error in the range.
- The acoustic signal may travel via the seafloor and then pipeline, then into the receiver (multipath). In this case, the direction of arrival from the pipeline will be correct (i.e. correct bathymetric height).
- Behind the pipeline, there is a shadow zone. The length of this zone is dependent on the exposure of the pipeline and the topography in the zone.

A more thorough treatment of the problem requires a study of scattering of acoustic waves from geometrical shapes with varying smoothness [15], [16]. In this paper, we consentrate on a more phenomenological description from a sensor observation point of view.

A fundamental question to be answered is if this particular pipeline produces non-specular reflection when observed with a HISAS type sonar. To potentially answer this, we consider a single ping. Figure 10 shows a sectorscan image (or a 2D phased array image of one ping). The pipeline is at approximately 163 m range. Note that the sonar broadside is not perpendicular to the pipeline. The image is constructed using standard delay-and-sum [12] with a Kaiser 3.5 array tapering to suppress sidelobes [17]. This to ensure that sidelobes from the specular reflection is not confused with the scattering off the specular direction. Figure 11 shows the relative backscattering strength from the pipeline, based on the same data as in Figure 10. The small oscillations in the backscattering strength is due to the sidelobes in the radiation pattern. The theoretical angular resolution of the phased array is

$$\beta = \frac{\lambda}{L} = \frac{1}{80} \approx 0.7^\circ.$$

We see that the backscattering strength from the pipeline is maximum at around $\theta_{sp} = -3.5^\circ$ off broadside at the direction for specular reflection. The directivity pattern for the transmitter and the receiver is not compensated for. This effect

Dette er en postprint-versjon/This is a postprint version.
DOI til publisert versjon/DOI to published version: 10.1109/OCEANSSYD.2010.5603518

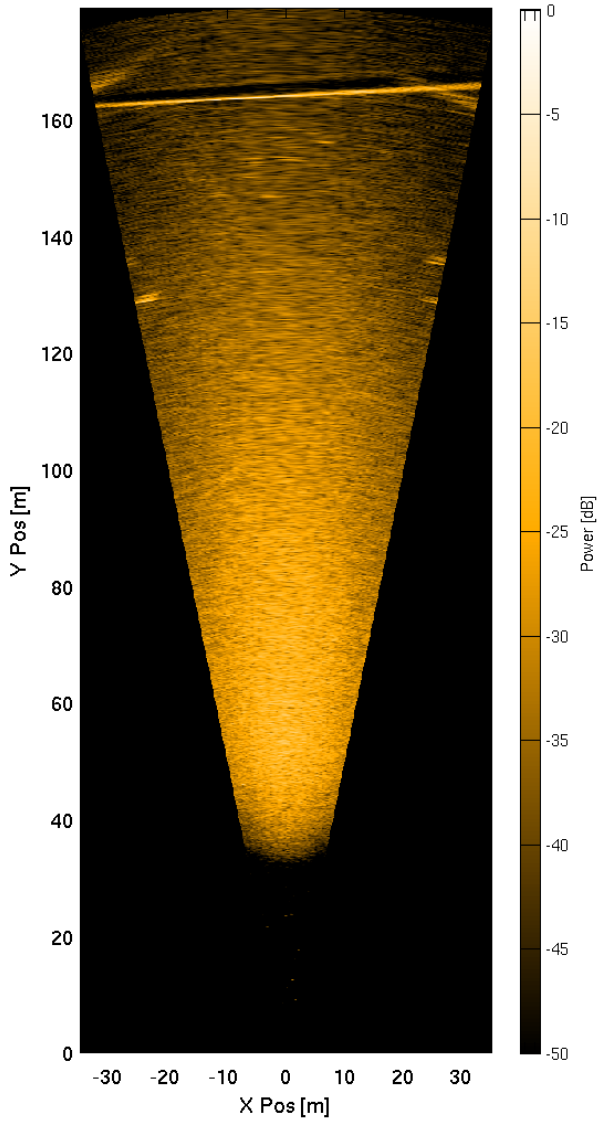


Fig. 10. Sectorscan image (phased array 2D image of one ping). The pipeline is at approximately 163 m range.

is, however, weak, compared with the observed results. The backscattering strength falls off in both directions off $\theta_{sp}$, as expected, but not very dramaticly. This indicates that there is a substantial amount of backscatter in the non-specular horizontal direction. This can be caused by two different effects:

- The pipeline has small scale roughness causing diffuse scattering
- The signal is specularly reflected via the pipeline through a bottom bounce – multiple reflections.

## V. Tracks parallel to the pipeline

In this section we consider two mission lines (or tracks) in Area B in Figure 5: One track west of the pipeline with an approximate range of 59 meters to the pipeline and one track east of the pipeline at a range of approximately 61 meters. Both tracks are close to parallel to the pipeline with an altitude of approximately 25 meters. Figure 6 shows one of the sidescan images from a parallel track to the pipeline.

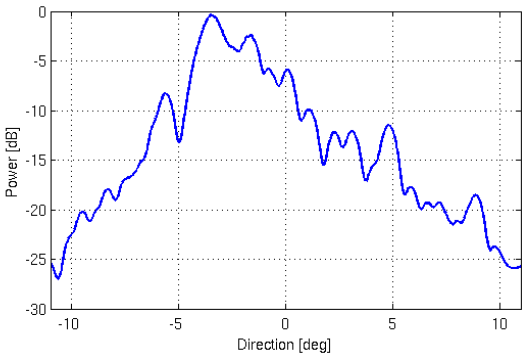


Fig. 11. Relative backscatter from the pipeline as function of angle.

For tracks parallel with the pipeline *specular reflection*, *shadowing* and *multipath* becomes important (see section IV). Specular reflection gives a strong reflection exactly perpendicular to the surface of the pipe. This reflection is the first echo from the pipeline in the image and gives a very distinct indication of the position of the pipeline. Note that if the pipeline is non-parallel with the vehicle track, as is the case in Figure 10, then specular reflection is not normal to the SAS-track.

Figure 12 shows example SAS images from a section of the pipeline. In the upper left panel, the pipeline observed from east and in the upper right panel the pipeline is observed from west. Note the changed location of the shadow behind the pipeline. The lower (large) panel shows the fusion of the images from each side (see section V-A).

### A. Co-registration details

The specular reflections from the pipeline occur in different locations when observed from the two different sides (see Figure 12). Thus, co-registering the two images [14] has to be based on other features. We have used five locations on the rope seen below the pipeline to manually co-register the images. In addition to an alignment, we had to apply a 0.4 degrees rotation of one of the images. In our study, we did not apply scaling, since the effect in this case is insignificant. The lower panel of Figure 12 shows the intensity-averaged combined image of the pipeline. By examining the rope we see that the images are successfully co-registered, almost everywhere. There are two visible errors in the fusion, circled out in Figure 13(c). These errors are probably due to a projection error due to an uncompensated error in the elevation of the rope.

### B. Characterisation of the pipeline

By measuring the range to the pipe, $R$, the height of the sensor relative to the seafloor (at the pipeline location), $H$, and the length of the shadow, $r$, we can estimate the height

Dette er en postprint-versjon/This is a postprint version.
DOI til publisert versjon/DOI to published version: 10.1109/OCEANSSYD.2010.5603518

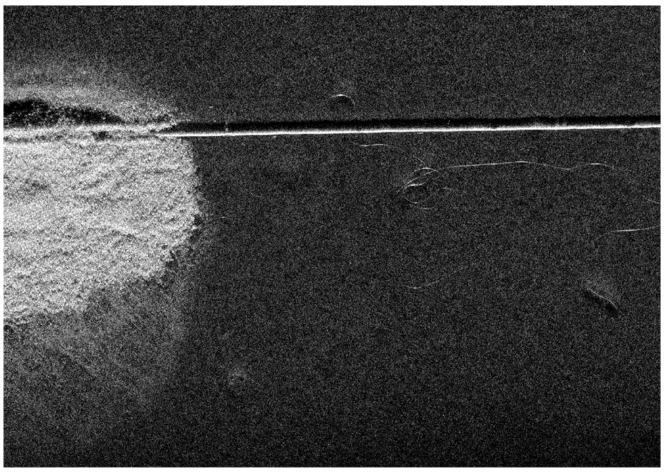

(a) SAS image from the east track

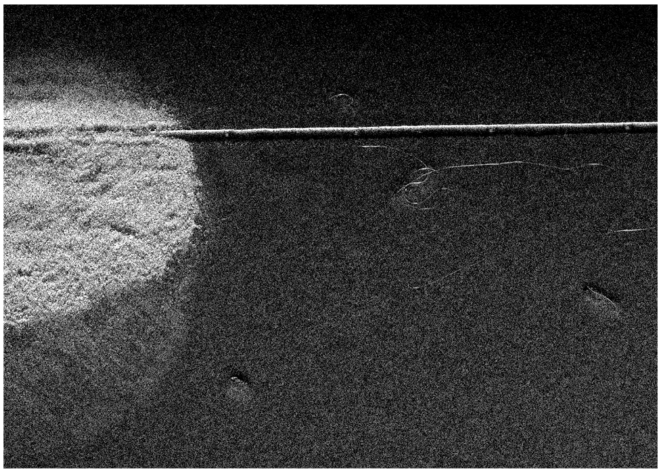

(b) SAS image from the west track

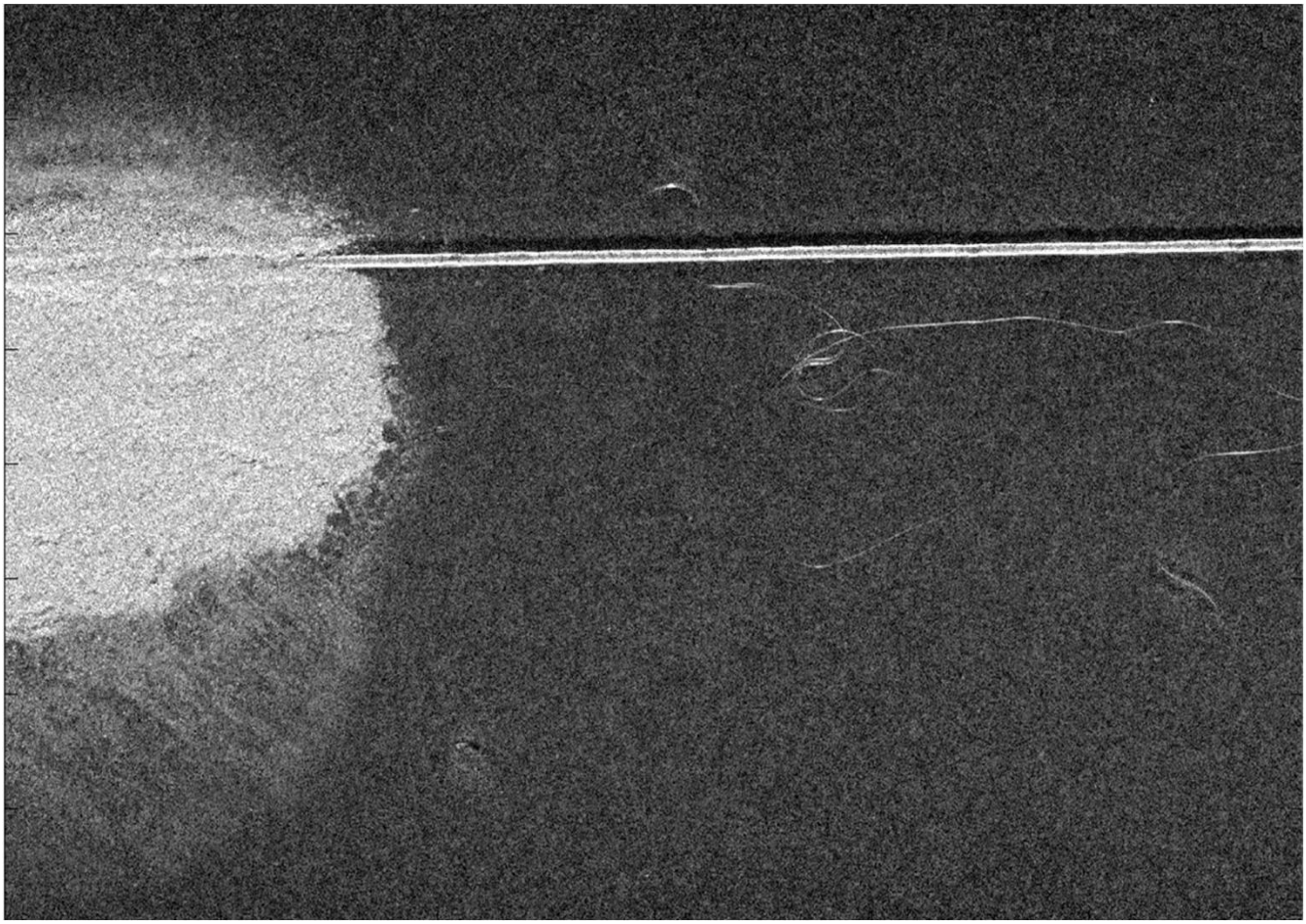

(c) SAS image merged from east and west track

Fig. 12. All panels shows SAS images from the same 60 by 40 meters on the seafloor. The AUV has run along the x-axis and range is along the y-axis. The two upper panels show the image from the east and west tracks respectively. The lower panel shows the result of merging the east and west tracks on an intensity basis.

Dette er en postprint-versjon/This is a postprint version.
DOI til publisert versjon/DOI to published version: 10.1109/OCEANSSYD.2010.5603518

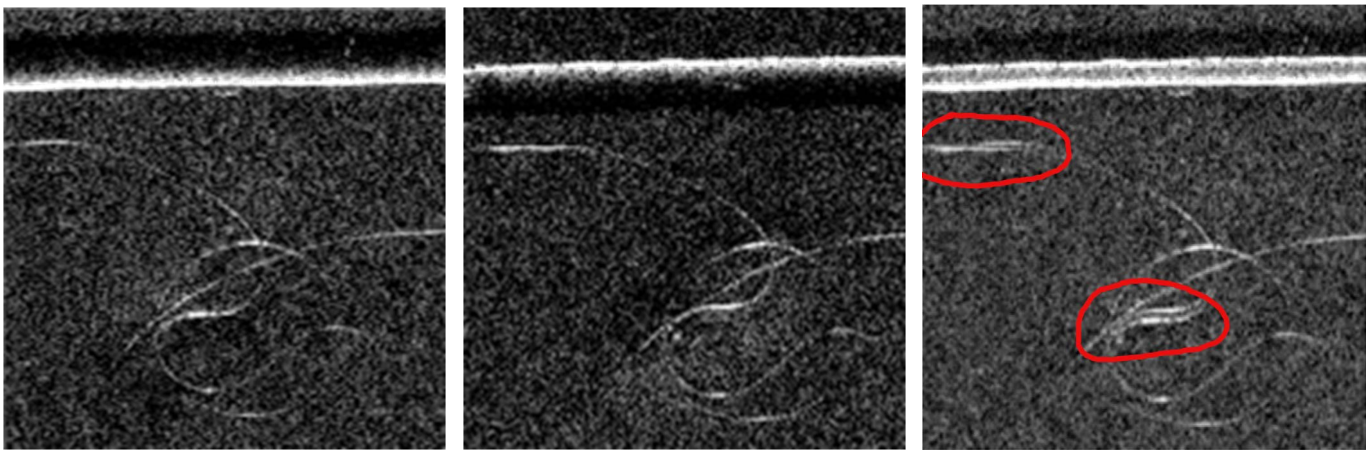

(a) SAS imagery from the east track (b) SAS imagery from the west track (c) SAS imagery merged from east and west track

Fig. 13. SAS image cutout containing the pipeline and the rope. Note the incorrect fusion of the rope on two places indicated in the right panel. This is due to an uncompensated elevation of the rope.

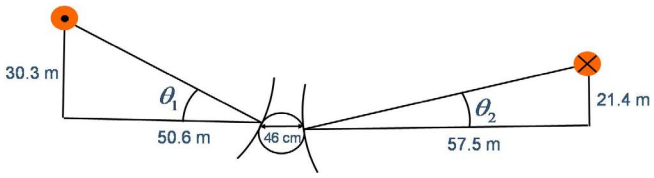


Fig. 14. Geometry of a two-sided pipeline survey. The orange circle at the upper left section is the AUV travelling out of the paper and the one at the upper right illustrates the AUV traveling into the paper. The measured width between the specular reflections, $w$, is equal to 46 cm.

of the pipeline relative to the seafloor, $h$

$$h = \frac{Hr}{R+r}. \tag{1}$$

This is a common method to estimate height of small objects with sidescan sonar [18].

We have estimated the height of the pipeline relative to the seafloor in a number of representative locations and found that it is typically elevated 29 cm. The actual pipeline has a diameter of 30 cm. The method is, however, not entirely conclusive. The bathymetry in the shadow causes uncertainty, and the burial of the pipeline is unknown.

In the combined SAS image in Figure 12(c), we see that the the pipeline has a certain width. By assuming that the first arrival is from the specular reflection in the vertical plane in both sides, the diameter $d$ can be approximated from the width $w$ of the pipeline

$$d \approx \frac{2w}{\cos\theta_1 + \cos\theta_2}, \tag{2}$$

where $\theta_1$ and $\theta_2$ are the incident angles to the pipeline relative to the sonar (see Figure 14). By averaging the estimate over 30 meters we find that $d \approx 46$ cm. The actual pipeline diameter was 30 cm. The reason for this discrepancy may be related to the error in the combined interferometry (see the next subsection).

### C. Combined Interferometry

We have applied the same co-registering technique on the interferometric estimates. Figure 15 shows the estimated bathymetry of the same region of the pipeline combined from two sides. The two sides are combined by selecting the region of maximum coherence [19] in the two single-look bathymetries, i.e. there is no averaging of the estimates. We removed a 27 cm vertical bias between the two bathymetries to get a smooth surface. This is most likely caused by inaccurate navigation or tidal changes causing an apparent depth change. Note that the combined SAS interferometry of the pipeline does not have the form of a cylinder – it appears flat at the center. This indicates that there is little backscatter from the top of the pipeline, or in the non-specular direction (see section IV).

## VI. Track perpendicular to the pipeline

In this section, we study data from Area A in Figure 5, where the AUV track is perpendicular to the pipeline. The sonar look-direction is then parallel to the pipeline. Specular reflection, shadowing and multipath is not dominant (as it was in the previous section, where the vehicle track was parallel to the pipeline). In this case, diffuse scattering (or backscattering in the non-specular direction) becomes important.

Figure 16 shows the estimated bathymetry from the starboard sonar (upper panel) along with the SAS image rendered onto the bathymetry (lower panel). The pipeline can be clearly seen in both panels. Note that the pipeline shape is more cylindrical compared to what we got from the parallel tracks. In the SAS image we see the pipeline joints as dark regions every 12.5 meters. These rather substantial differences in interferometric response are discussed further in the following sections.

Dette er en postprint-versjon/This is a postprint version.
DOI til publisert versjon/DOI to published version: 10.1109/OCEANSSYD.2010.5603518

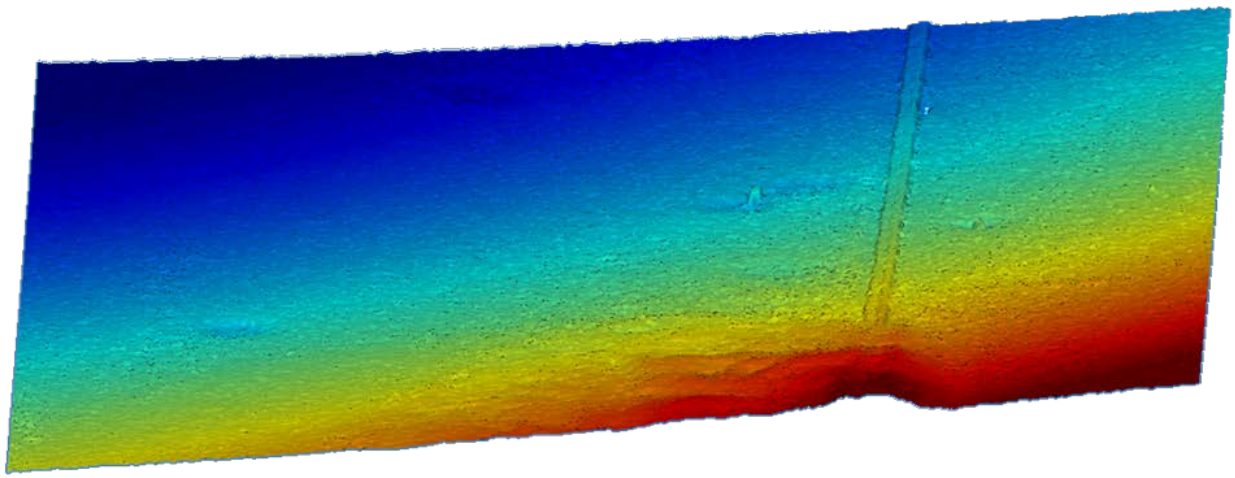

Fig. 15. Interferometric bathymetry from the same region as imaged in Figure 12. The bathymetry is combined from two tracks by selecting the side with the highest coherence for each pixel. Note the small elevated feature on the left side of the pipeline. This is part of the rope.

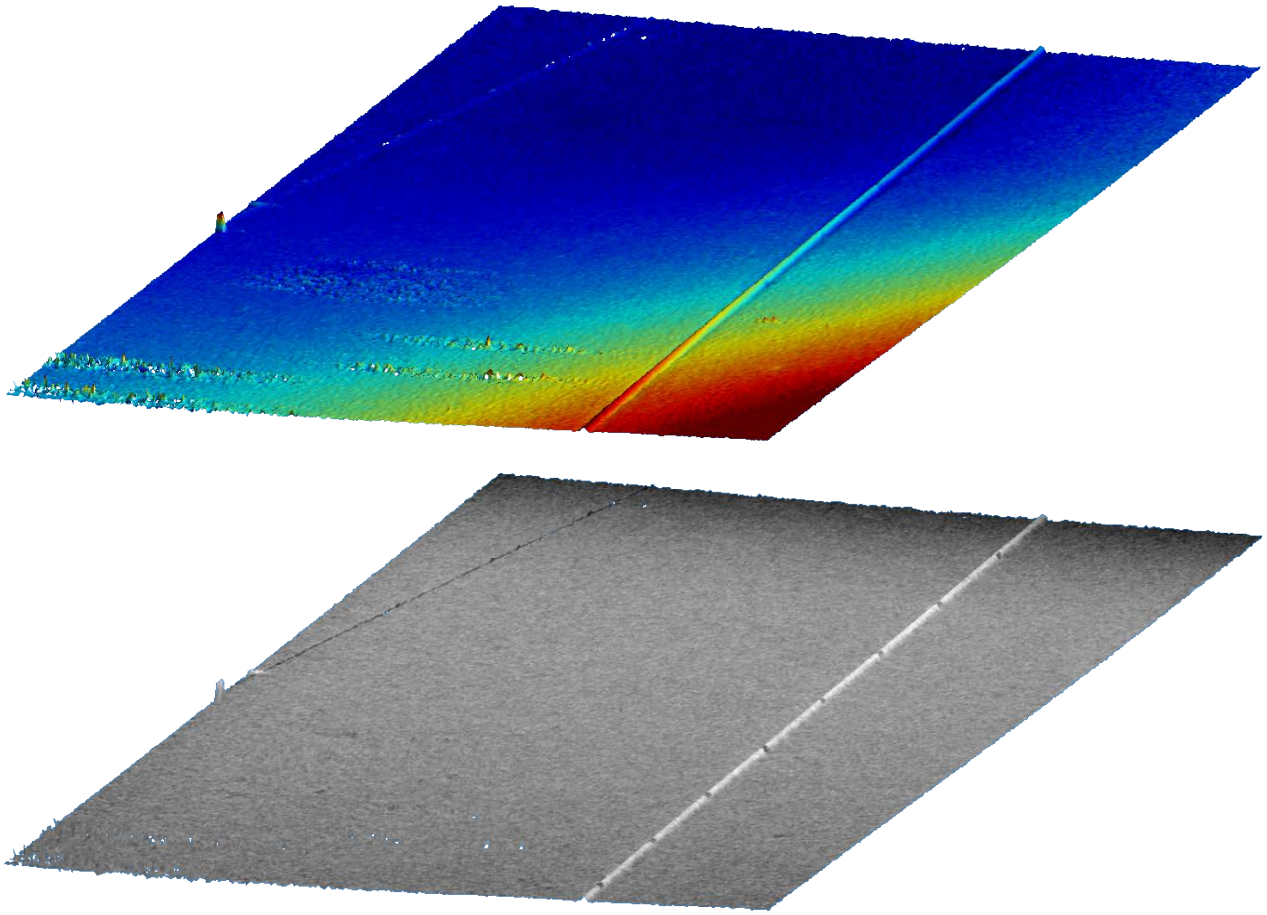

Fig. 16. A 100 meter section of the pipeline seen from a track perpendicular to the pipeline. The upper panel shows the interferometric bathymetry and the lower panel shows the SAS image rendered onto the bathymetry.

Dette er en postprint-versjon/This is a postprint version.
DOI til publisert versjon/DOI to published version: 10.1109/OCEANSSYD.2010.5603518

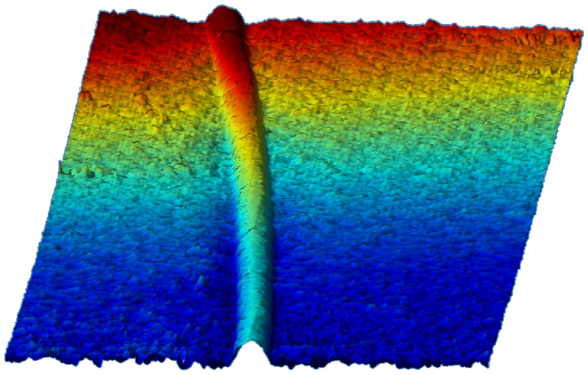

Fig. 17. A 8 by 100 meter zoom of a 100 meter section of the pipeline bathymetry in Figure 17. Note that the aspect ratio is not equal in the horizontal plane. The relative height of the pipeline is approximately 30 cm.

## VII. Estimating the shape of the pipeline

In the two previous sections we showed that the data collected from parallel and perpendicular tracks to the pipeline have very different characteristics. In this section we investigate these differences further.

Figure 17 shows a 8 by 100 meter cut-out from the data in Figure 16. By selecting the local maximum we can detect and track the peak of the pipeline, which gives the 3D position of the pipeline. This can be used to measure the local curvature of the pipeline.

The peak location can also be used to shift the bathymetry data in such a way that the pipeline is aligned along one axis. After linear detrending the local slope of the seafloor we can then average the bathymetry over the 100 metres, to get an estimate over the pipeline profile. The left panel of Figure 18 shows the estimated pipeline profile after shifting, detrending and averaging. The observed shape can intuitively seem to be a slight mismatch to a cylindrical pipeline, but this is actually as theory would predict:

- The interferometric estimate is not true 3D, but rather 2.5D - there is only one height at each horizontal position. This is due to the sensor geometry – the vertical receiver antenna is a sparse array containing only two elements, thereby only one measurement can be done.
- We apply a window of 9 by 9 image-samples to produce one interferometric estimate [20]. This is done to reduce variance in the height esimate. In effect, the bathymetry is lowpass filtered with an 18 cm window.

The measured height of the pipeline relative to the surrounding in the left panel of Figure 18 is around 30 cm, which fits with the diameter of the pipeline. The burial of the pipeline is unknown. We also tried to estimate the diameter based on the curvature of the profile, but due to the lowpass filtering, the profile is not cylindrical and the estimate varied from 33 to 40 cm depending on where we measured.

We have also performed similar analysis on the SAS image and averaged the intensity data to get a profile of the pipeline. The estimated width (and thereby diameter) varied from 30 to 57 cm depending on whether we measured -3 dB or -10 dB from the peak. This result is somewhat expected as the main lobe width of the imaging system is specified as 2.5 cm at -3 dB but wider at -10 dB.

In the right panel of Figure 18 we see an estimate of the pipeline profile from the merged bathymery data using the parallel tracks. We have applied the same shifting and averaging method as described above to produce the profile. The profile show several important features: Firstly, it is clear that the profile is dominated by the two specular reflections. Since the AUV height is different for the two tracks (see Figure 14) the specular reflections are at different heights. They are also smeared in range due to the interferometric window. Secondly, It seems that there is little echo from the top of the pipeline. There are some energy at the center of the pipeline profile, but the height is not above the specular reflections. Thirdly, there are energy below the seafloor surface, which indicates that we receive a multipath bounced onto the seafloor before it is echoed back into the sonar.

## VIII. Summary and future work

In this paper we have showed preliminary results from a pipeline survey using HUGIN 1000-MR AUV with the HISAS 1030 inteferometric SAS. We have focused on two different sections of the pipeline, one where the AUV tracks were parallel to the pipeline on each side and one where the track was perpendicular to the pipeline.

In the parallel tracks the pipeline is easily identifiable. The backscattered field is affected by specular reflection, shadowing and multipath. These features is also present in the interferometric data, but the estimated bathymetry is still usable to separate the pipeline from the rest of the seafloor. The shadowing can be eliminated by merging the data from two sides. The bathymetric pipeline profile does not fit a cylindrical shape, as expected, since the interferometric bathymetry estimate is dominated by the specular reflection.

In the track perpendicular to the pipeline, the pipeline is easily distinguished the rest of the seafloor, both in the SAS images and in the interferometric data. The bathymetric profile of the pipeline looked more like a lowpass filtered cylindrical object.

From the results we have presented it is clear that a HISAS 1030 interferometric SAS can be used to get useful information from a pipeline and its surroundings. The high resolution imagery and bathymetry of the seafloor is ideal for locating small objects in the proximity of the pipeline. At the pipeline the data are less intuitive – due to several acoustic effects which complicate the interpretation.

We have found that it may be beneficial to observe the pipeline not only from parallel tracks, which is most efficient, but also from perpendicular tracks. This can valuable information not easily retrievable otherwise. Whether this is worth the cost of increased survey time is left to further investigation.

Regarding the possible tasks in a pipeline inspection survey, we conclude that interferometric SAS, and HISAS 1030 in particular, can be used in:

Dette er en postprint-versjon/This is a postprint version.
DOI til publisert versjon/DOI to published version: 10.1109/OCEANSSYD.2010.5603518

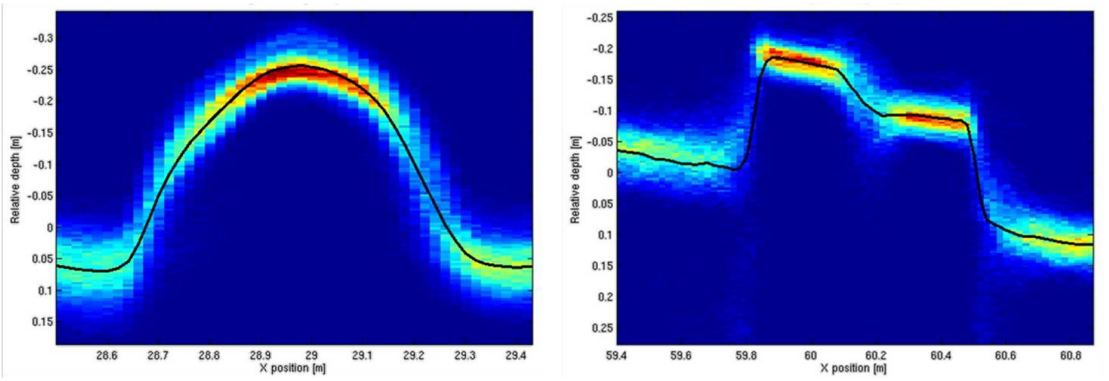


(a) Estimated pipeline profile from the perpendicular track

(b) Estimated pipeline profile from the parallel tracks

Fig. 18. Pipeline profile estimated by tracking the pipeline peak in the bathymetry, shifting and aligning the pipeline, detrending the local slope of the seafloor and averaging the bathymetry. The left panel show the results from the perpendicular track. The data is from a 100 meter section of the bathymethy showed in Figures 16 and 17. The right panel shows the result from the merged bathymetry of the parallel tracks. The data is from a 60 meter section of the bathymetry shown in Figure 15. The black line is the mean profile, while the colors indicates the distribution of points at each location. Red means a large number of samples at that location and blue means a low number of samples.

- Detection of burial and exposure of pipelines.
- Accurate estimation of the height of the pipeline above the surrounding seafloor, which can be used to indicate a free span.
- Detection of larger damages of pipelines - the detail level in SAS images is very high.
- Detection of buckling of pipelines.
- Excellent capability of detection of debris near the pipeline with large efficiency.

FFI and Kongsberg Maritime contiues to work with concepts of using autonomous underwater vehicles equipped with several sensors in pipeline inspection. We have an ongoing project to develop realtime tracking of pipelines, and we continue to develop methods and techniques in high resolution SAS imagery and interferometry for various applications such as pipeline inspection.

## ACKNOWLEDGMENTS

The authors thank the Royal Norwegian Navy and Helge Telle in particular, for the collection of the experimental data. The authors also thank Øivind Midtgaard and Stig A V Synnes at FFI for fruitful discussions. Finally, we thank Jan Arvid Ingulfsen at DOF Subsea for valuable input on pipeline inspection.

## REFERENCES

[1] H. D. Griffiths, T. A. Rafik, Z. Meng, C. F. N. Cowan, H. Shafeeu, and D. K. Anthony, "Interferometric synthetic aperture sonar for high-resolution 3-D mapping of the seabed," *IEE Proc. Radar, Sonar Navig.*, vol. 144 (2), pp. 96–103, 1997.

[2] P. E. Hagen and R. E. Hansen, "Area coverage rate for synthetic aperture sonars," in *Oceans '07 Europe*, Aberdeen, Scotland, June 2007.

[3] T. G. Fossum, T. O. Sæbø, B. Langli, H. J. Callow, and R. E. Hansen, "HISAS 1030 - high resolution interferometric synthetic aperture sonar," in *Proceedings of the Canadian Hydrographic Conference and National Surveyors Conference*, Victoria, BC, Canada, May 2008.

[4] P. E. Hagen, N. Størkersen, B.-E. Marthinsen, G. Sten, and K. Vestgård, "Rapid environmental assessment with autonomous underwater vehicles - examples from HUGIN operations," *Journal of Marine Systems*, vol. 69, pp. 137–145, 2008.

[5] R. E. Hansen, T. O. Sæbø, H. J. Callow, P. E. Hagen, and E. Hammerstad, "Synthetic aperture sonar processing for the HUGIN AUV," in *Proceedings of Oceans '05 Europe*, Brest, France, June 2005.

[6] R. Gauer, A. McFadzean, and C. Reid, "An automated sidescan sonar pipeline inspection system," in *OCEANS '99 MTS/IEEE*, Seattle, WA, USA, September 1999, pp. 811–816.

[7] Y. Petillot, S. Reed, and J. . Bell, "Real time auv pipeline detection and tracking using side scan sonar and multi-beam echo-sounder," in *OCEANS '02 MTS/IEEE*, Biloxi, MS, USA, October 2002, pp. 217–222.

[8] P. E. Hagen, T. G. Fossum, and R. E. Hansen, "HISAS 1030: The next generation mine hunting sonar for AUVs," in *UDT Pacific 2008 Conference Proceedings*, Sydney, Australia, November 2008.

[9] M. P. Bruce, "A processing requirement and resolution capability comparison of side-scan and synthetic-aperture sonars," *IEEE J. Oceanic Eng.*, vol. 17, no. 1, pp. 106–117, 1992.

[10] X. Lurton, *An Introduction to Underwater Acoustics: Principles and Applications*. London, UK: Springer Praxis Publishing, 2002.

[11] R. E. Hansen, J. Groen, and H. J. Callow, "Image enhancement in synthetic aperture sonar," in *Proceedings of Detection and Classification of Underwater Targets*, Edinburgh, UK, September 2007.

[12] D. H. Johnson and D. E. Dudgeon, *Array Signal Processing: Concepts and Techniques*, ser. Signal Processing Series. Englewood Cliffs, NJ, USA: Prentice Hall, 1993.

[13] R. F. Hanssen, *Radar Interferometry: Data Interpretation and Error Analysis*. Dordrecht, The Netherlands: Kluwer Academic Publishers, 2001.

[14] J. C. V. Jakowatz, D. E. Wahl, P. H. Eichel, D. C. Ghiglia, and P. A. Thompson, *Spotlight-Mode Synthetic Aperture Radar: A Signal Processing Approach*. Dordrecht, The Netherlands: Kluwer Academic Publishers, 1996.

[15] L. Brekhovskikh and Y. Lysanov, *Fundamentals of Ocean Acoustics*, ser. Springer Series in Electrophysics. Berlin, Germany: Springer-Verlag, 1982, vol. 8.

[16] J. A. Ogilvy, *Theory of Wave Scattering from Random Rough Surfaces*. Institute of Physics Publishing, 1991.

[17] F. J. Harris, "On the use of windows for harmonic analysis with the discrete fourier transform," *Proceedings of the IEEE*, vol. 66 (1), pp. 51–83, 1978.

[18] S. Reed, Y. Petillot, and J. Bell, "Automated approach to classification of mine-like objects in sidescan sonar using highlight and shadow information," *ieersn*, vol. 151, pp. 48–56, 2004.

[19] G. Franceschetti and R. Lanari, *Synthetic Aperture Radar Processing*. Boca Raton, FL, USA: CRC Press, 1999.

[20] T. O. Sæbø, H. J. Callow, R. E. Hansen, B. Langli, and E. O. Hammerstad, "Bathymetric capabilities of the HISAS interferometric synthetic aperture sonar," in *Proceedings of the OCEANS 2007 MTS/IEEE*, Vancouver, Canada, October 2007.

Dette er en postprint-versjon/This is a postprint version.
DOI til publisert versjon/DOI to published version: 10.1109/OCEANSSYD.2010.5603518